Journal of Power Sources 264 (2014) 220–228

Contents lists available at ScienceDirect

Journal of Power Sources

journal homepage: www.elsevier.com/locate/jpowsour

Single-chamber solid oxide fuel cells with nanocatalyst-modified anodes capable of *in situ* activation

Guangming Yang [a], Chao Su [a,b,*], Wei Wang [a], Ran Ran [a], Moses O. Tadé [b], Zongping Shao [b]

[a] State Key Laboratory of Materials-Oriented Chemical Engineering, College of Chemistry & Chemical Engineering, Nanjing Tech University, No. 5 Xin Mofan Road, Nanjing 210009, China
[b] Department of Chemical Engineering, Curtin University, Kent Street, Bentley, Perth, WA 6845, Australia

HIGHLIGHTS

- *In situ* activation of single-chamber SOFCs is realized using CH_4–O_2 mixture.
- Impregnation method was applied for preparing nanocatalysts-modified anodes.
- High power densities and OCVs were obtained for nanocatalysts-modified cells.
- CeO_2 nanoparticles in the anode retained similar morphology after the test.
- CeO_2 was the best choice for the single-chamber SOFC anode modification.

ARTICLE INFO

Article history:
Received 27 February 2014
Received in revised form
18 April 2014
Accepted 20 April 2014
Available online 28 April 2014

Keywords:
Single-chamber
Solid oxide fuel cell
In situ activation (initialization)
Nanocatalyst
Impregnation

ABSTRACT

Practical applications of single-chamber solid oxide fuel cells (SC-SOFCs) are partially limited by the difficulties and complications associated with the initialization process, which mainly involves the reduction of NiO to Ni in the anode. Here we propose a facile approach to the *in situ* activation (initialization) of SC-SOFCs with a state-of-the-art sintered nickel-based anode using a methane–oxygen gas mixture, combined with the introduction of nanocatalysts into the anode. RuO_2, CeO_2 or Co_3O_4 with the high activity for methane oxidation are investigated for above purpose. XRD results demonstrate that the nanocatalysts are successfully introduced into the anode *via* a simple solution impregnation technique. Using FESEM, different nanoparticle morphologies are observed for the three catalysts. The time dependence of the cell voltage operating on the methane–oxygen gas mixture demonstrates successful activation following nanocatalyst introduction. Single cells with different nanocatalyst-modified anodes, initialized by *in situ* reduction, deliver high open circuit voltages of approximately 1.0 V and significant peak power outputs of approximately 1000 mW cm^{-2} at a furnace temperature of 650 °C. XRD and FESEM analysis indicates that only the CeO_2 retains a same structure and morphology after the test. It suggests that the CeO_2 nanocatalyst is the most promising for practical applications.

1. Introduction

Single-chamber fuel cells (SCFCs), also called mono-chamber fuel cells, are distinguished from other types of fuel cells by their unique cell configuration, *i.e.*, the cells are operated in a sealing-free mode in which a fuel-oxidant gas mixture is applied as the atmosphere for both electrodes and where the structure is assembled in a single-gas chamber [1,2]. The operating principle of SCFCs relies on the different catalytic activity and selectivity of each electrode toward the gas mixture [3]. Although low-temperature fuel cells, such as polymer electrolyte membrane fuel cells, are sometimes operated in a single-chamber mode [4], significant safety concerns exist, because such configurations require hydrogen as the fuel, and the direct mixing of hydrogen and oxygen is extremely dangerous. Thus, single-chamber solid oxide fuel cells (SC-SOFCs) are attracting the most attention from researchers at present, because these configurations can use significantly more stable hydrocarbons as their fuel sources [5].

In comparison to the conventional dual-chamber SOFCs, SC-SOFCs allow rapid heating and cooling, simple cell and stack configurations, and simplified gas delivery systems. Therefore, SC-

* Corresponding author. Department of Chemical Engineering, Curtin University, Kent Street, Bentley, Perth, WA 6845, Australia. Tel.: +61 892669709; fax: +61 892662681.
E-mail address: chao.su@curtin.edu.au (C. Su).

http://dx.doi.org/10.1016/j.jpowsour.2014.04.091
0378-7753/

SOFCs are promising for applications as portable power sources, although some doubts regarding the practical application of SCFCs have also arisen among the community, in light of the typically poor fuel efficiency of this design. Today, SC-SOFCs have attracted new interest for the co-generation of electricity and chemicals from fuels, which offer the advantages of insensitivity to the polarization current and zero emission, compared to the conventional dual-chamber SOFCs [6,7]. This development solves the problem of using low-fuel-efficiency SC-SOFCs as sole power generating units, because all of the energy that is not converted to electricity by the SC-SOFCs can be stored in chemicals.

Until recently, research activities on SC-SOFCs have been mainly focused on cell performance improvement and the optimization of micro-fabrication processes, while a critical application step of SC-SOFCs, *i.e.*, the activation (initialization) process, has been overlooked [8–13]. Here, activation (initialization) means the creation of the electrocatalytic and catalytic activities of the anode toward the fuel-oxidant mixture through the *in situ* reduction of inert NiO in the anode to metallic Ni [14]. Because the fabrication of SOFCs is typically performed in air, the nickel in the anode is in an oxidized state, leaving almost no activity for the partial oxidation of hydrocarbons to syngas (a mixture of CO and H_2), as well as the electrochemical oxidation of H_2, CO and hydrocarbons; further, only small electronic conductivity of the anode remains. Hence, the anode should be reduced to achieve successful operation for power generation applications. In the dual-chamber configuration, the activation step is very simple, where diluted hydrogen is introduced into the anode chamber at relatively low temperatures to allow for the reduction of nickel oxide to metallic nickel in a gentle way. The hydrogen does not impact the stability of the cathode if the fuel cell sealing is perfect, however, for the SC-SOFCs, because both electrodes are located in the single-gas chamber, the *in situ* reduction of the anode with highly reducing hydrogen gas also results in the reduction of the cathode [14]. Previously, we proposed the *ex situ* reduction of NiO to Ni before depositing the cathode layer over the anode/electrolyte half-cell [15]. To avoid the re-oxidation of metallic Ni to NiO, calcination of the cathode layer should be performed in an inert atmosphere to establish sufficient mechanical strength. The need for a controlled atmosphere inevitably increases the complexity of cell fabrication and, thus, the capital cost, making SC-SOFCs less attractive for practical applications. Additionally, the use of an organic additive in the cathode precursor, which is added to prepare a proper slurry for painting onto the electrolyte surface, could create a local reducing atmosphere around the cathode during firing in inert atmosphere. Thereby, partial or even deep reduction of the cathode could still result. Thus, it would be preferable for the fuel cells to be *in situ* initialized by the same fuel-oxidant gas mixture for operation in a single-chamber mode.

Recently, we have demonstrated the realization of such *in situ* activation by depositing a Ru–CeO_2 catalyst layer onto the anode surface [16]. The catalyst converted the CH_4–O_2 gas mixture to a highly reducing syngas (H_2 and CO), which diffused into the anode layer to successfully reduce NiO to Ni, while the oxygen partial pressure near the cathode surface was similar to the methane–oxygen gas mixture as a result of the very poor catalytic activity of the cathode toward the partial oxidation of methane; consequently, the phase structure of the cathode material survived during the activation process. However, the Ru–CeO_2 catalyst layer was delaminated from the nickel-based anode after experiencing repeated thermal and redox cycling [17]. Additionally, this layer displayed poor conductivity, introducing additional drawbacks with respect to current collection.

During the past decade, nanostructured materials have received significant attention for their potential application in a wide range of fields due to their unique properties, which include a large specific surface area, excellent catalytic activity, high adsorption capacity, enhanced cell photochemical inversion rate, etc. [18–21]. Recently, the application of nanostructured materials in SOFCs to improve cell performance has also been exploited, and some progress has been made [22–26]. For example, Zhan et al. reported a SOFC using nanoscale Ni anode prepared by an impregnation method, which exhibited a low anode polarization resistance, as well as significantly improved cell performance measurements [26]. Impregnation is a common method for the introduction of nanoparticles into the porous electrodes of SOFCs.

In this study, we reported that the *in situ* initialization of SC-SOFCs with conventional sintered nickel cermet anode by a methane–oxygen gas mixture was readily realized by modifying the sintered anode with a nanocatalyst, such as RuO_2, CeO_2 or Co_3O_4, which was introduced by a solution impregnation method. The influence of the nanocatalyst on the SC-SOFC initialization process, the cell performance, and the morphological change after the performance test was investigated and is discussed systematically.

2. Experimental

2.1. Cell fabrication

Anode substrates, composed of commercial NiO (Chengdu Shudu Nano-science, China) and $(Y_2O_3)_{0.08}(ZrO_2)_{0.92}$ (YSZ, Tosoh), were prepared using a tape-casting process. To prepare the anode slurry for the tape-casting process, NiO, YSZ, starch (as a pore former) and triethanolamine (as a surfactant) were first ball-mill mixed at the mass ratio of 60:40:10:3 with a mixture of ethanol and dimethylbenzene for 24 h. Second, polyvinyl butyral (as a binder), polyethylene glycol (as a plasticizer) and dibutyl *o*-phthalate (as a plasticizer) with the mass ratio of 14:10:13 were added to the slurry, and then, the slurry was ball milled again for another 24 h. Then, the slurry was cast onto a tape after vacuum pumping to remove the air, and the cast slurry was allowed to dry in air overnight. Finally, the anode substrates were detached from the tape and were then drilled to form disks with diameters of 16 mm. The disks were then calcined at 1100 °C for 2 h to create sufficient mechanical strength. Next, a thin-film YSZ electrolyte layer was deposited onto each anode substrate *via* a wet powder-spraying technique. The anode/electrolyte half-cells were then sintered at 1400 °C for 5 h in air. Finally, a $Ba_{0.5}Sr_{0.5}Co_{0.8}Fe_{0.2}O_{3-\delta}$ (BSCF) cathode synthesized by using an EDTA-citric acid complexing sol–gel process was sprayed over the central surface of the electrolyte, giving an effective area of 0.48 cm^2, and each cell was fired at 850 °C for 2 h in air.

The nanocatalyst-modified anode was prepared using a solution impregnation method. A solution of either $Ce(NO_3)_3$, $RuCl_3$ or $Co(NO_3)_3$ was employed as the precursor of CeO_2, RuO_2 or Co_3O_4 nanocatalyst, respectively, at the concentration of 0.5 mol L^{-1}; this solution was impregnated into the unreduced NiO–YSZ anode scaffolds using a manual syringe. For each catalyst, three impregnation steps were performed to ensure sufficient catalyst. The loading of the infiltrated nanocatalysts (CeO_2, RuO_2 or Co_3O_4) was 3 wt.% in the porous NiO–YSZ scaffold. Each impregnation step was followed with a sequence of drying, slow heating to 500 °C at 2 °C min^{-1} and a dwell time of 30 min in air.

2.2. Activation test

The fuel cell was placed in a single-chamber reactor, and then the CH_4–O_2 gas mixture (CH_4: 200 mL min^{-1}, O_2: 100 mL min^{-1} [Standard Temperature and Pressure, STP]) was switched on. The

furnace temperature was increased to 650 °C at a rate of 30 °C min^{-1}, and then a dwell step was performed at 650 °C until the open circuit voltage (OCV) of the cell reached a stable value. The OCVs of the cells were monitored using a digital sourcemeter (Keithley 2420).

2.3. Characterization

The phase structures of the various anodes were analyzed using X-ray diffractometer (XRD, Bruker D8 Advance) with filtered Cu $K\alpha$ radiation ($\lambda = 0.154056$ nm). The scans were conducted in the 2θ range from 20 to 90° at room temperature. The morphologies of the anodes were examined using field-emissions scanning electron microscopy (FESEM, Hitachi S-4800). The cell performance test was conducted in a home-built electrochemical workstation. The *I–V* polarization curves of the cells were collected with a digital sourcemeter (Keithley 2420) that was based on a four-probe configuration.

3. Results and discussion

3.1. Basic properties of electrodes after impregnation

Impregnation is a facile method for the modification of porous scaffolds with functional materials, and this approach has been widely applied for the preparation of composite electrodes in SOFCs [27–30]. Such electrodes usually deliver superior performance in terms of activity and stability, and are better matched in terms of the thermal expansion behavior with other cell components, compared with composite electrodes prepared by a conventional physical mixing method. To successfully impregnate active materials into the electrode, the preparation of a highly porous scaffold is key. In this study, NiO–YSZ anode substrates with high porosity (approximately 30%) were readily fabricated from a combination of starch, used as a soft sacrifice pore former, and the tape-casting technique commonly invoked for anode fabrication.

Fig. 1 shows the XRD patterns of the anodes impregnated with different catalysts after calcination at 800 °C. The XRD pattern of the fresh anode substrate used for impregnation is also presented for comparison purposes; this pattern is readily indexed based on a physical mixture of NiO and fluorite YSZ phases. For the anode impregnated with $Ce(NO_3)_3$ post-calcination, in addition to the basic diffraction peaks of NiO and YSZ phases, diffraction peaks at approximately 33.1, 47.6 and 56.4° can be observed, which are indexed as the (2 0 0), (2 2 0) and (3 1 1) diffraction planes of fluorite-type cubic CeO_2, respectively by comparison with standard cubic CeO_2 (Joint Committee on Powder Diffraction Standards, JCPDS card No. 01-0800). This finding suggests that the porous anode was successfully modified with the CeO_2 catalyst. Similarly, Co_3O_4 and RuO_2 phases were observed in the XRD patterns of the anodes impregnated, respectively, with $Co(NO_3)_3$ and $RuCl_3$ after calcination. The above results demonstrate the effective incorporation of the targeted phases into the anode scaffolds.

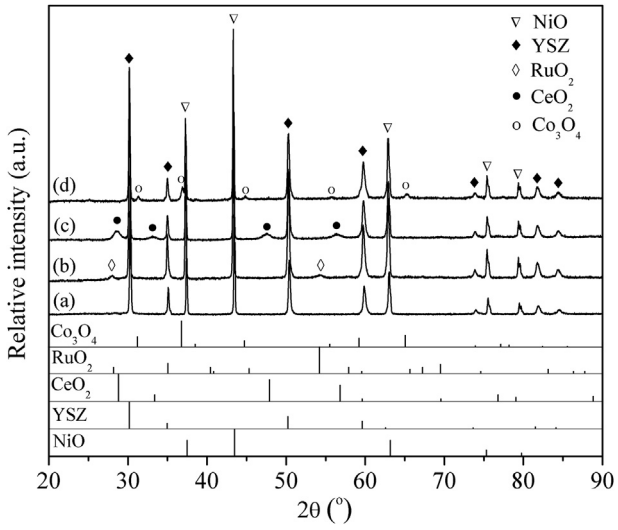

Fig. 1. XRD patterns of the fresh NiO–YSZ anode (a) and the anodes modified with RuO_2 (b), CeO_2 (c) and Co_3O_4 (d). Cubic NiO (JCPDS card No. 01-1239), cubic YSZ (No. 30-1468), tetragonal RuO_2 (No. 18-1139), cubic CeO_2 (No. 01-0800) and cubic Co_3O_4 (No. 09-0418) from the JCPDS database are shown for comparison.

The morphologies of the anodes after impregnation were examined by FESEM. For comparison, the FESEM image of the NiO–YSZ anode is also shown in Fig. 2. Due to the presence of starch as the pore former and the application of other organic additives during the tape casting step, as expected, a significant porosity fraction was obtained, even though the NiO–YSZ anode was sintered at the high temperature of 1400 °C (Fig. 2(a)), however, the NiO and YSZ particles were poorly sintered, yielding grain sizes in the range of several micrometers. For the anode modified with RuO_2, cylindrical nanoparticles were observed over the anode surface, with diameters of approximately 100–200 nm (Fig. 2(b)). It is well known that rutile-structured RuO_2 single crystals usually take the cylindrical shape [31]. This result implies that the cylindrical particles in the impregnated anode substrate were the RuO_2 phase. For the anodes modified with CeO_2 or Co_3O_4, obvious nanoparticles were detected over the two anodes surfaces (Fig. 2(c) and (d)), although their respective morphological shapes varied slightly. The particles decorated the anode surfaces, significantly increasing the surface roughness of the anode. The particle sizes were approximately 80 and 20 nm for Co_3O_4 and CeO_2, respectively. The CeO_2 nanocatalyst was more concentrated in terms of particle distribution, relative to the Co_3O_4 catalyst.

3.2. Activation process

Completed cells, *i.e.*, cells with the configuration of (anode) nanocatalyst-impregnated Ni–YSZ|YSZ|BSCF (cathode), were used to test the capability of the nanocatalyst-modified anodes for *in situ* initialization with the CH_4–O_2 gas mixture in the single-chamber mode. For reasonable comparison, a cell with a pre-reduced Ni–YSZ anode and a cell with an unreduced NiO–YSZ anode were also tested. All of the anode-supported thin-film electrolyte bi-layer cells were fabricated from the same batch to minimize any differences in cell microstructure. Previously, the BSCF cathode was typically fired at temperatures of 950 or 1000 °C when SDC was applied as the electrolyte. In this study, a firing temperature of 850 °C for the BSCF cathode was chosen based on two considerations. First, BSCF has a high reactivity with YSZ, becoming significant at temperatures higher than 900 °C [32,33]. Second, the high-temperature calcination can result in the nanocatalyst sintering as deposited over the anode [34]. To ensure that the cathode still possesses sufficient mechanical strength and good adhesion to the electrolyte surface, the BSCF slurry was prepared using high-energy ball milling, which reduced the BSCF particle size, thus increasing the sintering ability of the system. To perform the *in situ* activation step, the CH_4–O_2 gas stream was introduced in parallel with the fuel cell disk. It is worth noting that gas phase reaction between CH_4 and O_2 can take place at high temperatures, leading to the formation of H_2 and CO, which are highly reductive and could cause anode reduction and cathode reduction. To minimize the effect of gas phase reaction on the reduction of the fuel cell electrode, the

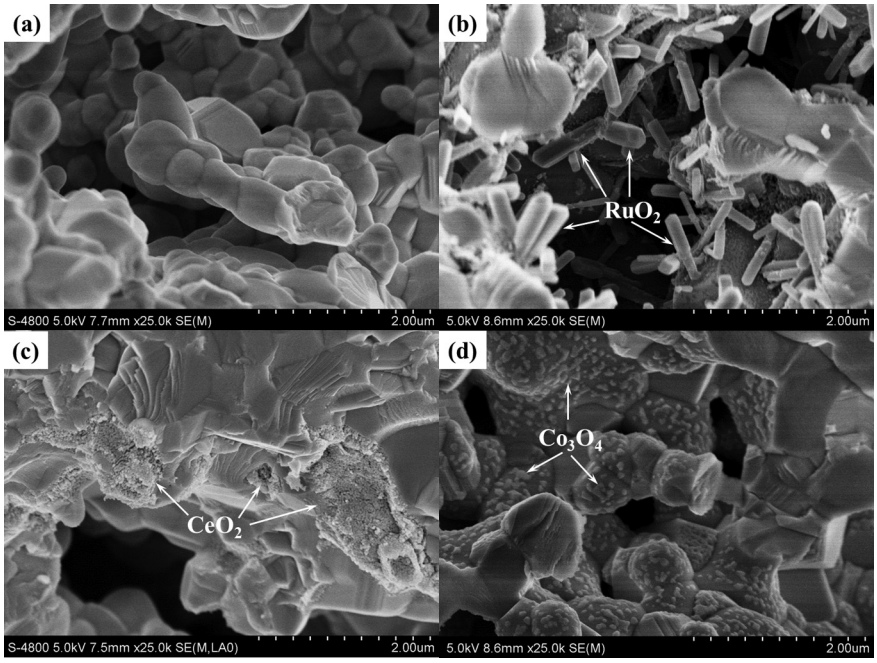

Fig. 2. FESEM images of the fresh NiO–YSZ anode (a) and the anodes modified with RuO_2 (b), CeO_2 (c) and Co_3O_4 (d).

highest temperature used for the *in situ* initialization of the anode was 650 °C.

The fuel cell is actually an oxygen concentration differential cell, and its OCV is determined by the difference in the oxygen potential over the cathode and anode surfaces. Because of the poor activity of BSCF with respect to methane partial oxidation and combustion at intermediate temperatures, the oxygen potential over the cathode surface can be considered the same as that of the surrounding atmosphere ($CH_4 + O_2$), while the oxygen potential over the anode surface is strongly determined by the catalytic activity of the anode toward the partial oxidation of methane. As shown in Fig. 3(a), for the cell with the pre-reduced Ni–YSZ anode, when the furnace temperature was lower than 480 °C, the fuel cell still showed low OCVs (<0.2 V), suggesting poor activity of the reduced sintered nickel cermet anode for either the partial oxidation of methane to syngas or the deep oxidation of methane at low temperatures. A rapid increase in the cell OCV was observed at a furnace temperature of approximately 500 °C, indicating that the reduced anode started to have high activity for methane conversion, thus resulting in a sharp decrease in the oxygen partial pressure at the anode surface. As to the non-impregnated cell with the unreduced anode, the OCV was held lower than 0.1 V for temperatures up to 650 °C, denoting the failure of the *in situ* reduction of the anode by the CH_4–O_2 gas mixture. After the test, the anode remained green in color, which is the original color of a fresh NiO–YSZ anode. The anode surface resistance was readily measured using a digital multimeter at room temperature, which displayed an infinite value, further demonstrating that the anode was not *in situ* reduced, as shown in Fig. 4(a), where "1" represents the out-of-range value.

For the cells with anodes modified by various nanocatalysts (RuO_2, CeO_2 and Co_3O_4), successful initialization was demonstrated by the high and stable OCVs recorded after operating with the CH_4–O_2 gas mixture at 650 °C for a certain period of time. In comparison to the pre-reduced anode, the OCV of the nanocatalyst-modified cells increased more gently during the initialization process, which can be explained by the progressive reduction of the NiO to Ni in the anode. The gentle initialization process is actually a good character for maintaining the integrity of the fuel cell, because the slow reduction of the anode mediates the internal strain associated with the volume change that occurs following the reduction of NiO to metallic Ni. At temperatures lower than 480 °C, the cells with nanocatalyst-modified unreduced anodes showed higher OCVs than the cell with the pre-reduced Ni–YSZ anode. The nano-size RuO_2, CeO_2 and Co_3O_4 oxides all have high activities for methane activation (either partial oxidation or deep oxidation) [35–37], while the reduced Ni–YSZ mainly has activity for the partial oxidation of methane [38]. At temperatures lower than 480 °C, the reduced Ni–YSZ anode had relatively poor catalytic activity for the partial oxidation of methane, because the anode was severely sintered, thus the oxygen partial pressure at the anode remained high, resulting in low OCVs. Due to the high surface area of the nanocatalysts, the catalytic combustion of methane likely happened over the nanocatalyst-modified anodes at temperatures lower than 480 °C, consuming oxygen as a result and creating a low oxygen partial pressure over the anode surface; this led to a steady increase in the OCV. With respect to the anodes modified with the RuO_2 and Co_3O_4 nanocatalysts, the low oxygen partial pressure created from the deep combustion caused the reduction of RuO_2 and Co_3O_4, respectively, to metallic Ru and Co, which are highly active catalysts for the partial oxidation of methane [35,36]. Consequently, syngas was generated during the initialization process, causing the progressive reduction of NiO to Ni. Finally, the fuel cell anode was fully activated. The nano-size CeO_2 primarily behaved as a catalyst for the deep oxidation of methane [37], thereby consuming oxygen and creating a low local oxygen partial pressure over the anode surface. The oxygen potential over the anode surface could have been so low that it would have exceeded the stability window of NiO, inducing the decomposition of NiO to Ni. The metallic Ni formed as a result of this reduction then further promoted the conversion of oxygen *via* methane partial oxidation. Finally, the total activation of the fuel cell anode was realized. The successful activation of the nanocatalyst-modified anodes was further supported by the extremely low anode surface resistances values recorded, as seen in Fig. 4(b)–(d), where all of the resistance values were less than 1.0 Ω.

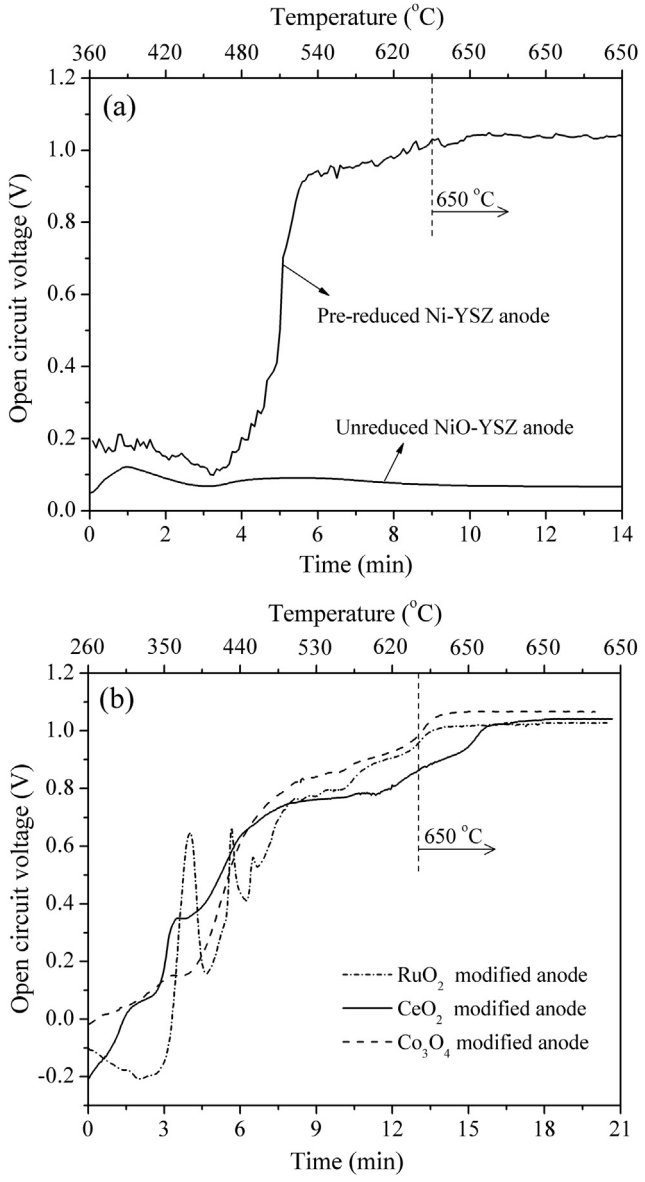

Fig. 3. The time dependence of OCV for the fuel cells with the pre-reduced Ni–YSZ anode, the unreduced NiO–YSZ anode (a), and the anodes modified with RuO_2, CeO_2 and Co_3O_4, respectively (b).

3.3. Cell performance

To demonstrate further the successful activation of the fuel cells with nanocatalyst-modified anodes in a mixture of CH_4–O_2 gas, cell performance tests were conducted by measuring the *I–V* polarization curves after the OCV reached the stable value at the activation temperature of 650 °C (furnace temperature). Fig. 5 presents the typical *I–V* polarization curves of the cells with the pre-reduced Ni–YSZ anode and the nanocatalyst-modified Ni–YSZ anodes when operating in a CH_4–O_2 gas mixture under different CH_4-to-O_2 ratios. The total flow rate was fixed at 300 mL min^{-1} [STP]. At all investigated CH_4-to-O_2 ratios, namely, from 1.0 to 2.0, favorable cell power outputs were observed for all four cells. For the conventional SOFC with the *ex situ* reduced nickel-based anode, peak power densities (PPDs) 310–1040 mW cm^{-2} were achieved at the furnace temperature of 650 °C. For the other three cells with anodes containing the RuO_2, CeO_2 or Co_3O_4 nanocatalyst, PPDs of 500–920, 830–1020 and 1000–1220 mW cm^{-2} were achieved, respectively. The significant power outputs strongly indicate the successful activation of the fuel cells (the reduction of NiO to Ni). For the partial oxidation of methane, the maximum syngas production was reported for the CH_4-to-O_2 ratios ranging from 1.8 to 2.0 [6,39], however, the best cell performance for all four cells was achieved at CH_4-to-O_2 ratios in the range of 1.0–1.5. Taking the fuel cell with the RuO_2-modified Ni–YSZ anode as an example, the PPD was approximately 500 mW cm^{-2} at a CH_4-to-O_2 ratio of 2.0 and increased to 630 mW cm^{-2} when the ratio was reduced to 1.75. The value was further increased to 920 mW cm^{-2} at a ratio of 1.25, but the PPD was reduced to 885 mW cm^{-2} with the further decrease of the CH_4-to-O_2 ratio to 1.0. It is well known that both partial and full oxidation of CH_4 are exothermic reactions. The addition of RuO_2, Co_3O_4 or CeO_2 nanocatalysts into Ni–YSZ anode can promote the reaction rate of partial/full oxidation of CH_4, resulting in a higher cell temperature than the furnace temperature during the operation of SC-SOFC. Different CH_4-to-O_2 ratios produce different amount of heat released in the exothermic reactions, thus, leading to different cell temperatures. To exploit the effect of the CH_4-to-O_2 ratio on the cell performance, the actual temperatures of cells under different CH_4-to-O_2 ratios at the furnace temperature of 650 °C were measured with the results shown in Fig. 6. It is apparent that the cells with nanocatalyst-modified anodes showed the higher cell temperature than the cell without the modification of nanocatalyst at all the investigated CH_4-to-O_2 ratios. Furthermore, the cell temperatures increased with decreasing CH_4-to-O_2 ratios, which interpreted the higher cell performance at the lower CH_4-to-O_2 ratio except the ratio of 1:1. It implies that the difference of actual cell temperatures at various CH_4-to-O_2 ratios is not the only reason for obtaining different cell performance. As we know, the cell performance was determined based on the performance of both the anode and the cathode. Many perovskite oxides also possess certain levels of activity for methane oxidation (mainly, deep oxidation) at elevated temperatures [40–42]. This reaction would partially consume the oxygen in the gas mixture, thus reducing the oxygen partial pressure in the atmosphere. The larger O_2-to-CH_4 ratio in the gas mixture would yield a higher oxygen concentration, and thus a lower cathodic polarization resistance would be achieved. However, increasing the O_2-to-CH_4 ratio in the fuel gas would reduce the syngas product rate, in addition to its concentration in the anode gas. As a result, increased anodic polarization resistance would be expected. It seems the CH_4-to-O_2 ratio of 1.0–1.5 resulted in the lowest sum of anode and cathode polarization resistances, yielding the best cell power output. A significant concentration polarization was observed at high polarization current densities for all cells, suggesting either insufficient oxygen supply for the cathode or syngas supply for the anode. This fact also could have resulted from a formation rate of syngas that was insufficient to match the syngas electrocatalytic oxidation rate. Such a concentration polarization at a high current density is typical for SC-SOFCs operating under CH_4–O_2 gas mixtures [6,43]. Regardless, very attractive power outputs were achieved for the *in situ* initialized fuel cells impregnated with nanocatalysts.

As mentioned, many perovskite oxides also possess a certain level of the catalytic activity necessary for the fuel oxidation reaction, for example, methane combustion. BSCF is known to possess modest activity for methane combustion reactions [40]. The conversion of CH_4 and O_2 over a perovskite oxide is strongly dependent on the space velocity [41,42]. Therefore, an increase in the space velocity of CH_4–O_2 gas mixture in a given SC-SOFC could lead to a decrease in the conversion of CH_4 and O_2 over the cathode side, resulting in a higher cathode performance relative to that expected. Fig. 7 shows the *I–V* polarization curves of the fuel cell with RuO_2 modified Ni–YSZ anode operating on various CH_4–O_2 gas mixtures

Fig. 4. The anode surface resistances of cells with the unreduced NiO–YSZ anode (a) and the NiO–YSZ anodes modified with RuO_2 (b), CeO_2 (c) and Co_3O_4 (d), after the initialization process.

at a fixed CH_4-to-O_2 ratio of 2:1 but with the total flow rate varied from 225 to 450 mL min^{-1} [STP]. The PPD increased monotonically with increasing total flow rate. The PPD was 420 mW cm^{-2} at a total flow rate of 225 mL min^{-1} and then increased to 640 mW cm^{-2} at a flow rate of 300 mL min^{-1}, and further increased to 790 mW cm^{-2} at 375 mL min^{-1} and then 900 mW cm^{-2} at 450 mL min^{-1}. This result strongly suggests that the relatively poor cathode performance limited the cell power output, particularly at high CH_4-to-O_2

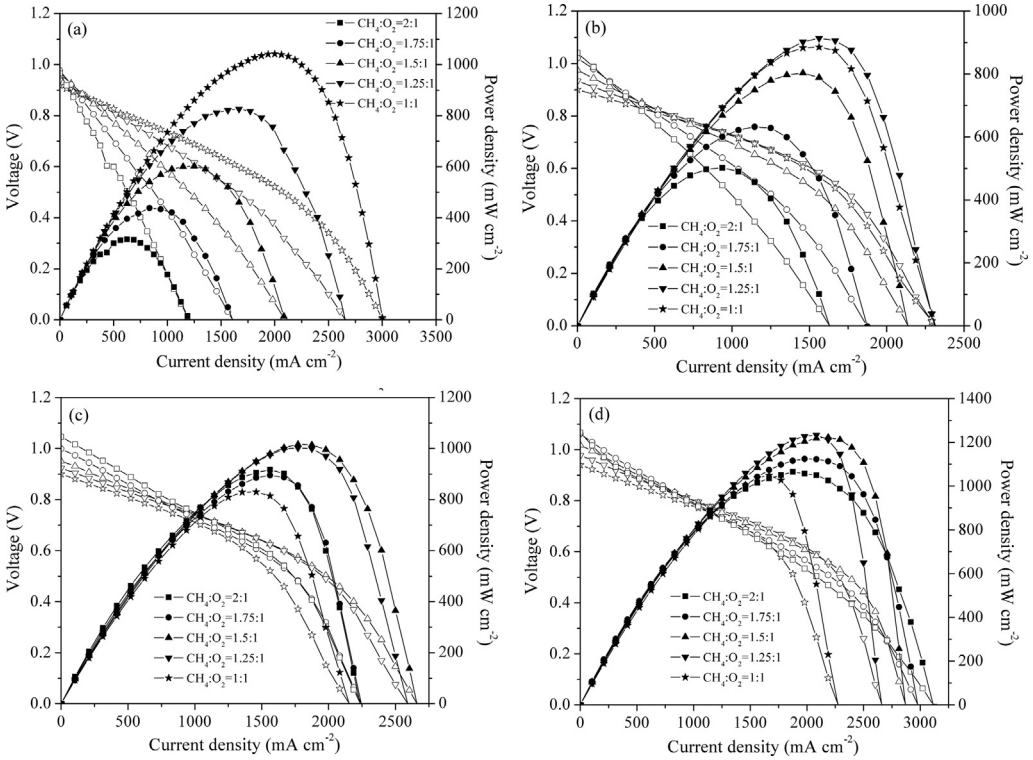

Fig. 5. The *I–V* and *I–P* curves of the fuel cells with the pre-reduced NiO–YSZ anode (a) and the NiO–YSZ anodes modified with RuO_2 (b), CeO_2 (c) and Co_3O_4 (d), operating under different ratios of a CH_4–O_2 gas mixture at the furnace temperature of 650 °C.

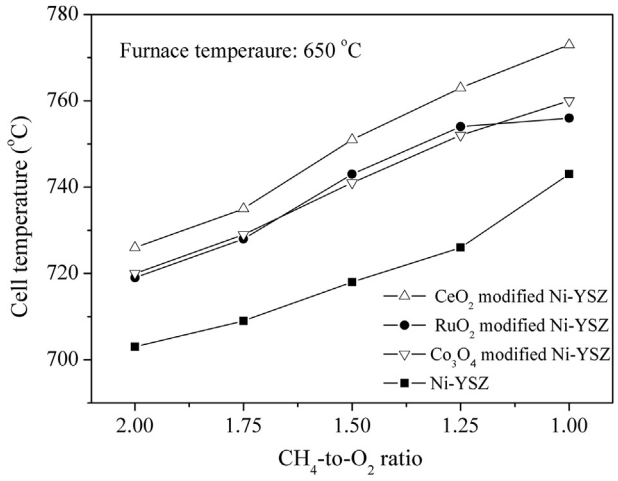

Fig. 6. The actual temperatures of the cells with different anodes under various CH_4–O_2 gas mixtures with different CH_4-to-O_2 ratios at the furnace temperature of 650 °C.

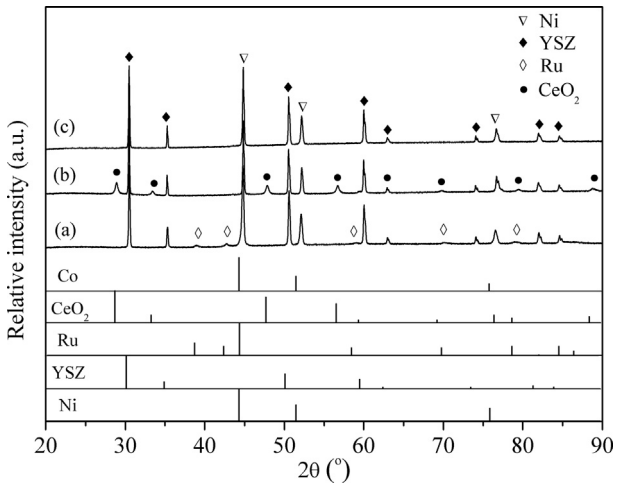

Fig. 8. XRD patterns of the anodes modified with RuO_2 (a), CeO_2 (b) and Co_3O_4 (c), after fuel cell activation and *I–V* polarization test. Cubic Ni (JCPDS card No. 01-1258), cubic YSZ (No. 30-1468), hexagonal Ru (No. 01-1256), cubic CeO_2 (No. 01-0800) and cubic Co (No. 15-0806) from the JCPDS database are shown for comparison.

ratios of the fuel gas and low total flow rates of the gas mixture. That is, the anode was sufficiently activated following *in situ* initialization by the CH_4–O_2 gas mixture.

3.4. Electrode structure and morphology after the activation process

How the nanocatalysts behaved after the *in situ* activation of the anodes at elevated temperatures (650 °C) is of interest to this study. For portable applications of SC-SOFCs, the devices must be capable of frequent on and off switching, which would likely subject the devices to frequent periods of cooling and heating. With decreasing operation temperature, the fuel cell anode starts to develop insufficient activity for the partial oxidation of the fuel, which can lead to the oxygen in the CH_4–O_2 gas mixture causing the re-oxidization of metallic Ni to NiO. That is, the anode may sometimes require multiple activation processes. High nanocatalyst stability is of substantial importance for realizing multiple activation processes; however, it is well known that nanomaterials usually have poor thermal stability due to their high surface energies. To examine the stability of anodes modified with various nanocatalysts, the anodes were subjected for XRD and FESEM characterization after

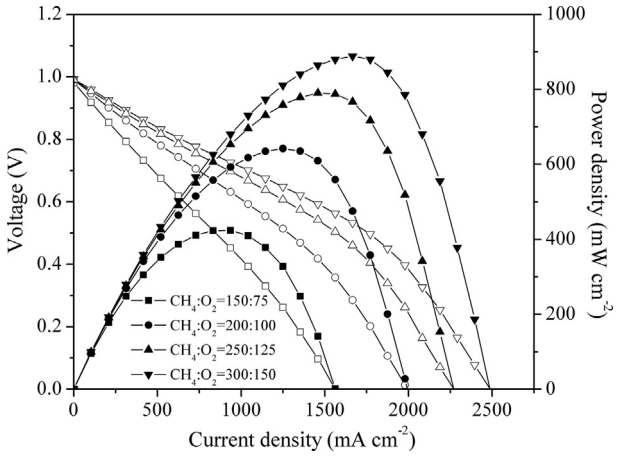

Fig. 7. The *I–V* and *I–P* curves of the fuel cell with the RuO_2 modified Ni–YSZ anode, operating under various CH_4–O_2 gas mixtures with different total flow rates at the furnace temperature of 650 °C.

conducting the fuel cell activation and the *I–V* polarization test at 650 °C for a couple of hours. As shown in Fig. 8, the CeO_2 phase still can be observed in the XRD pattern of the CeO_2-modified anode as compared with Fig. 1. As for the RuO_2-modified anode, the metallic Ru phase was observed while RuO_2 phase disappeared. It suggests the phase change from RuO_2 to Ru occurred after the activation and cell performance test. For the Co_3O_4-modified anode, only the basic diffraction peaks of Ni and YSZ phases were observed. The possible reason is that the diffraction peaks of metallic Co cannot be detected by the XRD due to the small amount of cobalt and almost identical diffraction peaks for metallic Ni and Co (both of them possess the face centered cubic structure). Furthermore, cobalt nanocatalyst was likely dissolved into the anode substrate for forming Ni–Co alloys because of the high reactivity of nanomaterials, which have a similar diffraction peaks with metallic nickel when the Co content is very low in the Ni–Co alloy [44–46]. Fig. 9(a) shows the FESEM of the anode modified with the RuO_2 nanocatalyst after the activation and performance test. The cylindrical RuO_2 was completely replaced by the amorphous nanoparticles, and significant nanocatalyst sintering was observed. In connection with the XRD results (Fig. 8), the amorphous nanoparticles are metallic Ru. For the CeO_2-modified anode, as shown in Fig. 9(b), the electrode morphology did not changed significantly, compared with the anode before the activation process (Fig. 2(c)). The CeO_2 nanoparticles survived over the anode surface, and particle sizes of 40 nm were observed after activation, which was grown somewhat to that before the activation of the anode. Fig. 9(c) shows the morphology of the Co_3O_4-impregnated anode after activation and the performance test, where the Co nanoparticles had almost disappeared. It further supported the formation of Ni–Co alloys. The SEM results are in good agreement with the XRD results (Fig. 8). Based on the above results, it is clear that the as-prepared CeO_2 nanoparticles had significantly higher thermal and chemical stabilities than RuO_2 and Co_3O_4, thus this catalyst is the most suitable among the three for realizing multiple *in situ* activations of SC-SOFCs using a gas mixture of CH_4–O_2.

4. Conclusions

In this work, the *in situ* initialization of SC-SOFCs is successfully realized by applying nanocatalyst-modified anodes prepared *via*

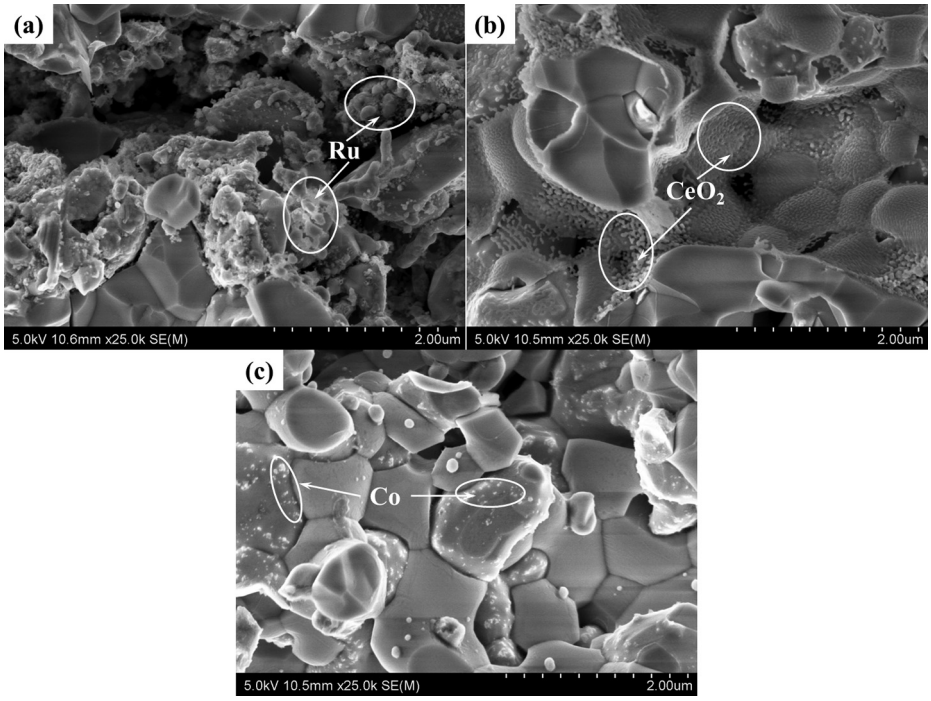

Fig. 9. FESEM images of the anodes modified with RuO_2 (a), CeO_2 (b) and Co_3O_4 (c), after fuel cell activation and *I–V* polarization test.

impregnation when operating on a CH_4–O_2 gas mixture. The nanocatalysts, namely, RuO_2, CeO_2 and Co_3O_4, possess high catalytic activities for the methane oxidation reaction, even at the low temperature of 450 °C, thereby facilitating the reduction of anode NiO into metallic Ni. At the furnace temperature of 650 °C, similar maximum power densities of approximately 1000 mW cm^{-2} and OCVs of approximately 1.0 V are achieved for the cells when using the different nanocatalysts (RuO_2, CeO_2 or Co_3O_4)-modified anodes, where these values are comparable to that of the cell with the pre-reduced anode. For all of the cells, the optimal ratio of CH_4 and O_2 in the CH_4–O_2 mixture feed for SC-SOFC operation is approximately 1.0–1.5, and the peak power density increases with increasing total flow rate of the mixture. In comparison with the fresh anodes modified with different nanocatalysts, the morphologies of the anodes after the activation process change significantly because of extensive nanocatalyst sintering, except for the anode with introduced CeO_2 nanoparticles. Therefore, the CeO_2 nanocatalyst is determined to be the best choice for SC-SOFC anode modification. This nanocatalyst can accomplish both the *in situ* activation of cells and excellent power outputs.

Acknowledgment

The authors acknowledge the support received from the Australian Research Council Future Fellowship under the contract of FT100100134.

References

[1] C. Eyraud, J. Lenoir, M. Gery, Compt. Rend. 252 (1961) 1599–1603.
[2] C.K. Dyer, Nature 343 (1990) 547–548.
[3] M.A. Priestnall, V.P. Kotzeva, D.J. Fish, E.M. Nilsson, J. Power Sources 106 (2002) 21–30.
[4] B.C.H. Steele, A. Heinzel, Nature 414 (2001) 345–352.
[5] M. Yano, A. Tomita, M. Sano, T. Hibino, Solid State Ionics 177 (2007) 3351–3359.
[6] Z.P. Shao, C.M. Zhang, W. Wang, C. Su, W. Zhou, Z.H. Zhu, H.J. Park, C. Kwak, Angew. Chem. Int. Ed. 123 (2011) 1832–1837.
[7] T. Tagawa, K.K. Moe, M. Ito, S. Goto, Chem. Eng. Sci. 54 (1999) 1553–1557.
[8] D. Rembelski, M. Rieu, L. Combemale, J.P. Viricelle, J. Power Sources 242 (2013) 811–816.
[9] I. Riess, J. Power Sources 175 (2008) 325–337.
[10] T. Hibino, A. Hashimoto, T. Inoue, J.I. Tokuno, S.I. Yoshida, M. Sano, Science 288 (2000) 2031–2033.
[11] B. Morel, R. Roberge, S. Savoie, T.W. Napporn, M. Meunier, J. Power Sources 186 (2009) 89–95.
[12] M.L. Liu, Z. Lü, B. Wei, X.Q. Huang, Y.H. Zhang, W.H. Su, Solid State Ionics 181 (2010) 939–942.
[13] C. Gaudillère, P. Vernoux, D. Farrusseng, Electrochem. Commun. 12 (2010) 1322–1325.
[14] C.M. Zhang, Y. Zheng, R. Ran, Z.P. Shao, W.Q. Jin, N.P. Xu, J. Ahn, J. Power Sources 179 (2008) 640–648.
[15] C.M. Zhang, Y. Zheng, Y. Lin, R. Ran, Z.P. Shao, D. Farrusseng, J. Power Sources 191 (2009) 225–232.
[16] C.M. Zhang, L.L. Sun, R. Ran, Z.P. Shao, Electrochem. Commun. 11 (2009) 1563–1566.
[17] W. Wang, C. Su, Y.Z. Wu, R. Ran, Z.P. Shao, J. Power Sources 195 (2010) 402–411.
[18] J. Jamnik, J. Maier, Phys. Chem. Chem. Phys. 5 (2003) 5215–5220.
[19] A.S. Arico, P. Bruce, B. Scrosati, J.M. Tarascon, W. Van Schalkwijk, Nat. Mater. 4 (2005) 366–377.
[20] Y.Y. Shao, J. Liu, Y. Wang, Y.H. Lin, J. Mater. Chem. 19 (2009) 46–59.
[21] J. Yang, J.B. You, C.C. Chen, W.C. Hsu, H.R. Tan, X.W. Zhang, Z.R. Hong, Y. Yang, ACS Nano 5 (2011) 6210–6217.
[22] J.M. Vohs, R.J. Gorte, Adv. Mater. 21 (2009) 943–956.
[23] Z.Y. Jiang, C.R. Xia, F.L. Chen, Electrochim. Acta 55 (2010) 3595–3605.
[24] S.P. Jiang, Mater. Sci. Eng. A 418 (2006) 199–210.
[25] G.M. Yang, C. Su, R. Ran, M.O. Tade, Z.P. Shao, Energy Fuels 28 (2014) 356–362.
[26] Z.L. Zhan, D.M. Bierschenk, J.S. Cronin, S.A. Barnett, Energy Environ. Sci. 4 (2011) 3951–3954.
[27] T.Z. Sholklapper, H. Kurokawa, C. Jacobson, S.J. Visco, L.C. De Jonghe, Nano Lett. 7 (2007) 2136–2141.
[28] X.B. Zhu, Z. Lü, B. Wei, Y.H. Zhang, X.Q. Huang, W.H. Su, Int. J. Hydrogen Energy 35 (2010) 6897–6904.
[29] Z.Y. Jiang, Z.W. Lei, B. Ding, C.R. Xia, F. Zhao, F.L. Chen, Int. J. Hydrogen Energy 35 (2010) 8322–8330.
[30] S.P. Jiang, Int. J. Hydrogen Energy 37 (2011) 449–470.
[31] S. Neupane, G. Kaganas, R. Valenzuela, L. Kumari, X.W. Wang, W.Z. Li, J. Mater. Sci. 46 (2011) 4803–4811.
[32] Z.S. Duan, M. Yang, A.Y. Yan, Z.F. Hou, Y.L. Dong, Y. Chong, M.J. Cheng, W.S. Yang, J. Power Sources 160 (2006) 57–64.
[33] D.J. Chen, G.M. Yang, Z.P. Shao, F. Ciucci, Electrochem. Commun. 35 (2013) 131–134.
[34] F.M. Courtel, H. Duncan, Y. Abu-Lebdeh, I.J. Davidson, J. Mater. Chem. 21 (2011) 10206–10218.
[35] I. Balint, A. Miyazaki, K.I. Aika, React. Kinet. Catal. Lett. 80 (2003) 81–87.

[36] L.H. Hu, Q. Peng, Y.D. Li, ChemCatChem 3 (2011) 868–874.
[37] W. Tang, Z.P. Hu, M.J. Wang, G.D. Stucky, H. Metiu, E.W. McFarland, J. Catal. 273 (2010) 125–137.
[38] C. Guerra, A. Lanzini, P. Leone, M. Santarelli, N.P. Brandon, J. Power Sources 245 (2014) 154–163.
[39] S.J. Ahn, Y.B. Kim, J. Moon, J.H. Lee, J. Kim, J. Power Sources 171 (2007) 511–516.
[40] Z.P. Shao, J. Mederos, W.C. Cheuh, S.M. Haile, J. Power Sources 162 (2006) 589–596.
[41] V.R. Choudhary, K.C. Mondal, Appl. Energy 83 (2006) 1024–1032.
[42] J. Hu, T.L. Xing, Q.C. Jia, H.S. Hao, D.L. Yang, Y.Q. Guo, X. Hu, Appl. Catal. A Gen. 306 (2006) 29–33.
[43] M.L. Liu, Z. Lü, B. Wei, X.Q. Huang, Y.H. Zhang, W.H. Su, J. Power Sources 195 (2010) 4247–4251.
[44] T. Yamauchi, Y. Tsukahara, K. Yamada, T. Sakata, Y. Wada, Chem. Mater. 23 (2011) 75–84.
[45] L.P. Wang, Y. Gao, Q.J. Xue, H.W. Liu, T. Xu, Appl. Surf. Sci. 242 (2005) 326–332.
[46] T. Syukri, Y. Ban, Y. Ohya, Y. Takahashi, Mater. Chem. Phys. 78 (2003) 645–649.